Conical Coordinates for Elliptical Orbits

Douglas H. May[1]
University of Arizona, Tucson, Arizona, 85721, USA

Two-body orbital motion is analyzed within a three-dimensional conical reference frame in which the center of the gravitational field is within the cone volume and the apex angle is fixed at 90 degrees. In this frame the satellite position is characterized by slant height R along the cone surface in addition to the classical radial distance r. The constraint of the cone half-angle being 45 degrees gives a line along the angular momentum vector to the cone apex with the magnitude of $\sqrt{ap}$, where a is the semi-major axis and p is the semi parameter. Three results are developed. First, the tilt angle Φ_h of the orbital plane relative to the cone axis satisfies $\sin(2\Phi_h) = e$, providing a direct geometric encoding of eccentricity that is intrinsic to the frame and requires no reference to the orbit. Second, applying Gauss's law for gravitation to the conical surface yields a logarithmic flux integral that is shown to be equivalent pointwise to Kepler's equation through the eccentric anomaly E, establishing a three-dimensional geometric interpretation of that classical result. Third, the logarithmic structure allows for a Newton-Raphson positioning method with dual convergence tolerances for both the Kepler residual and the position variable, offering geometric consistency and balanced numerical resolution throughout the orbit. This is especially useful for high-eccentricity cases.

I. Nomenclature

A, F, P	=	orbit apoapsis, ellipse prime focus, periapsis
S	=	satellite position
E	=	eccentric anomaly
R, R'	=	cone slant height, local conic circumference radius
a	=	semi-major axis
e	=	eccentricity
h	=	specific angular momentum
p	=	semi-parameter, semi-latus rectum
r	=	radius, radius vector
t	=	time
Φ	=	spherical and conic frame angle from the z axis
Θ	=	spherical and conic frame angle in the x–y plane
θ	=	true anomaly
μ	=	unique gravitational constant for the primary body
Φ_h	=	orbital plane tilt angle from cone axis, $\sin(2\Phi h) = e$
Φ_c	=	spherical cap half-angle
Ω	=	solid angle subtended by conic sector (steradians)
Ψ	=	gravitational flux through a surface
M	=	mean anomaly
λ	=	logarithmic position variable
$\boldsymbol{g}$	=	gravitational acceleration vector at Gaussian surface
$\boldsymbol{n}$	=	outward unit normal on Gaussian surface
τ_E, τ_λ	=	convergence tolerances for Kepler residual and logarithmic position increment

[1]Instructor, University of Arizona, Senior Engineering Design, AIAA Associate Fellow.

II. Introduction

Since ancient Greek times, mathematicians and astronomers have studied conic sections. Apollonius of Perga systematically developed the geometry of ellipses, parabolas, and hyperbolas around 200 BC.[1] It wasn't until 1609 that cone geometry was related to gravity and orbits when Kepler published his first law stating that planets orbit the sun on elliptical paths with the sun located at one focus. This relationship provided the basis for Kepler to match orbital data to planetary motion and publish his second law in the same year stating, "The line joining the planet to the sun sweeps out equal areas in equal times." His construction of a model gave the equation for position and time that remains important today. In 1619 Kepler published his third law which states, "The square of the period of a planet is proportional to the cube of its mean distance from the sun." These laws, combined with Newton's law of gravitation, establish the mathematical foundation for analyzing orbital motion in the plane of the orbit. [2, 3, 4]

Kepler's equation relates orbital position to time through an auxiliary circle and the eccentric anomaly E. His transcendental equation requires an iterative numerical solution, as no closed-form algebraic expression exists for E as a function of time. See Eq. (1). The traditional coordinate framework uses polar coordinates centered at the gravitational focus and treats orbital motion primarily as a planar phenomenon. This gives limited attention to how satellites interact with the three-dimensional nature of the gravitational field during their motion. [2, 3, 4]

$$\sqrt{\frac{\mu}{a^3}}\, t = E - e \sin E \tag{1}$$

Reference [5] derives Eq. (1) by rearranging the vis viva equation and integrating with respect to time. The derivation employs conservation of angular momentum and the vis viva energy equation, reproducing Kepler's equation through calculus methods and confirming that the traditional framework, however approached, constrains orbital mechanics to planar motion.

Derivation of Kepler's equation by the calculus method demonstrates that vectors are applicable until the dot product converts the equation to scalar energy values. Calculus yields the same result as Kepler's model and equation; however, both approaches limit the mechanics to planar motion. This paper adopts an alternative geometric framework, developed in Ref. [6] , for analyzing elliptical orbits in a conical reference frame with its apex notionally positioned at the center of a spherical field.[2] In this framework, the satellite's position is characterized by slant height R measured along the cone surface from the apex, in addition to the traditional radial distance r from primary body to satellite. A right circular cone with a 90-degree apex angle proves particularly advantageous; it eliminates position-dependent geometric terms and reveals direct algebraic relationships between orbital parameters.*

The conical framework offers new perspectives. A set of elliptical orbits sharing the same specific mechanical energy comprise a family of ellipses on a cone's surface, where each ellipse's eccentricity reflects its angle relative to the cone's axis. A fundamental geometric relationship emerges naturally between the radius vector r, and the slant height R. Orbital motion decomposes into rectilinear motion along the cone surface and rotation about the cone axis, revealing structure not apparent in traditional planar coordinates.

This analysis focuses on bound elliptical orbits and demonstrates three contributions within the conical framework. First, the tilt angle Φ_h of the orbital plane relative to the cone axis satisfies $\sin 2\Phi_h = e$, providing a direct geometric encoding of eccentricity without reference to the orbital plane. Second, applying Gauss's law for gravitation to the conical surface yields a logarithmic flux integral that connects pointwise to the eccentric anomaly throughout the orbit, establishing a three-dimensional geometric interpretation of Kepler's equation. Third, these results support a numerical positioning scheme with dual convergence tolerances, one on the Kepler residual and one on the logarithmic position variable that provides an independent geometric consistency check unavailable in the classical two-dimensional approach.

III. Three-Dimensional Coordinates

Gravitation from the center of a force field acts as the reciprocal of distance squared equally in all directions. Textbooks and publications typically begin analyses of orbital motion in the field with a description limited to the orbit and the satellite rotating in-plane about the primary body. Special case trajectories without a rotational component are rectilinear. Vallado notes that for each of the orbital geometrical shapes, a rectilinear special case results from the

---

* Published references agree closely on orbital mechanics nomenclature. This paper follows Curtis [3] in using θ for true anomaly. Bate, et al [2] and Vallado [4] uses v for the same quantity; v does not appear in this paper.

plane lying on the surface of the cone extending from the apex as a slant height of the cone. [4] Rectilinear trajectories contribute to orbital motion analyses mathematically. The following sections incorporate this unique motion.

With a spherical model, a body situated on the surface of a sphere with radius R experiences an attractive force towards the center of the sphere with the value $-\mu/R^2$. This is Newton's gravitational force equation as applied in orbital mechanics with μ as the gravitation constant, G, times the mass of the primary body. In this paper, the symbol R represents the distance from the origin (apex) in a conical coordinate system, while r refers to the distance between the two bodies in an orbital problem. Figure 1 shows a force field having spherical symmetry and a conical reference frame with its apex at the center of the sphere. In the spherical gravity force field, all vectors radiate from the center along linear paths. The conical reference frame has radii R along slant heights, or cone generators, on the surface of a right circular cone. For purely radial motion—objects falling directly toward or escaping directly from the primary body—this spherical coordinate system is natural and sufficient. However, for orbital motion with angular momentum, the satellite trajectory does not approach the origin, and the three-dimensional structure of its interaction with the gravitational field becomes relevant. The conical frame provides geometric structure that accommodates both the radial component of motion and the angular momentum constraint.

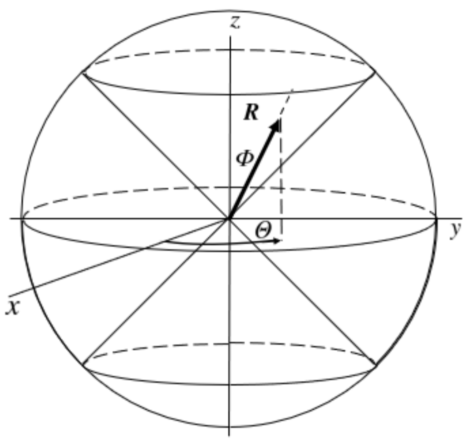

Fig. 1 Conic Reference Frame in a Spherical Field

Orbiting bodies trace paths that are conic sections. Since the early 1600s, this principle has been thoroughly tested mathematically and proven through real-world implementation. Having established spherical symmetry and the conic relationship, the cone is sufficient for further analysis in this paper. The next section describes variables in the conic frame.

IV. Geometry of Elliptical Orbits in a Conical Frame

A. Basic Geometry of Elliptical Orbits.

Figure 2 shows a general plane in a conical reference frame for an elliptical orbit. The model of the orbit within the plane that intersects the cone is unchanged from the classical two-dimensional reference frame. The radius vector r extends from the main body to the satellite, while θ represents the true anomaly angle measured from the periapsis. Apoapsis is at A and R is the slant height at the satellite's position. At a given distance from the apex, we construct OF perpendicular to the plane of the orbit. In Fig. 2, the area swept by the radius vector corresponds to Kepler's model. The conical reference frame is related to a Cartesian coordinate system (x, y, z) with the z-axis coinciding with the cone centerline. As shown in Fig. 3, the classical orbital parameters are applicable, and the conical parameters R, Φ, and Θ adequately specify the satellite's position.

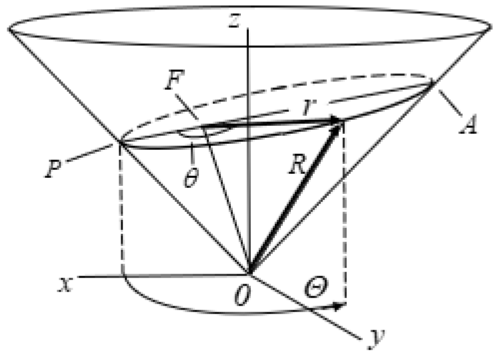

Fig. 2 Three-Dimensional Conical Reference Frame with Orbital Plane Intersection

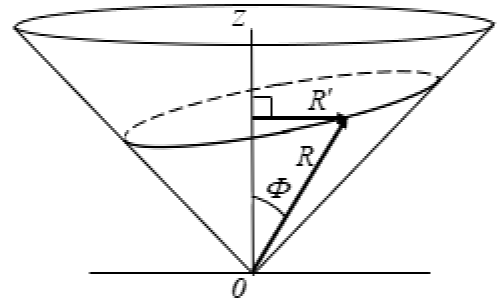

Fig. 3 The Component of *R* Perpendicular to the Cone Axis, *R'*

B. Edge View Analysis.

Reference [6] develops simplified algebraic relationships for an elliptical orbit in a cone with a preferred apex angle. Begin with *0F* having unknown length and construct the edge view shown in Fig. 4 with the line of apses in the plane of the paper and *0F* both perpendicular to the orbit plane and extending to the cone apex. Relate the right triangles in Fig. 4 to give a preferred value for the apex angle. Reference [6] presents the derivation from the edge view geometry. The result, simplified in Eq. (2), gives the preferred apex angle. Figure 4 shows the resulting edge view.

$$\overline{OF}^2 - 2\,\overline{OF}\,a\,cot(\alpha+\beta) - a^2(1-e^2) = 0 \tag{2}$$

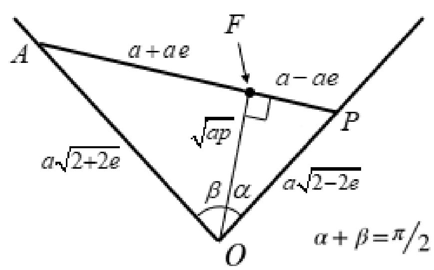

Fig. 4 Edge View After Solving for *α*, *β*, *OA*, and *OP*

Equation (2) and the reference frame simplify when $\alpha+\beta=\pi/2$, and line *OF* becomes $a\sqrt{1-e^2}=\sqrt{ap}$. This 90° apex angle is the central geometric result: it eliminates position-dependent terms from the frame and establishes the constant $\sqrt{ap}$ as both a geometric length and a physical quantity that is perpendicular to the orbit plane and collinear with the angular momentum vector ***h***.

C. The Fundamental Relationship.

With the cone apex angle fixed at 90°, the right triangle formed by R, r, and $\sqrt{ap}$ at any point in the orbit has the relationship:

$$R^2 = r^2 + ap \tag{3}$$

The quantity $\sqrt{ap}$ is an orbital constant for a given eccentricity, just as the total specific mechanical energy $-\mu/2a$ is constant.

D. Families of Elliptical Orbits.

A family of elliptic orbits with the same total energy but varying eccentricity can be described in the conical reference frame between the limiting cases of a circular orbit ($e = 0$) and a rectilinear trajectory ($e \to 1$). Figure 5 depicts this family from an edge view. All orbits in the family share the same major axis value, $2a$, and the conic section angle relative to the cone axis depends on the eccentricity. Within the spherical and conical reference frames described, we have upper and lower nappes of the conical geometry. An orbit in the upper nappe shown in Fig. 5 has an equivalent geometric construction in the lower nappe. The dotted lines display this equivalent configuration.

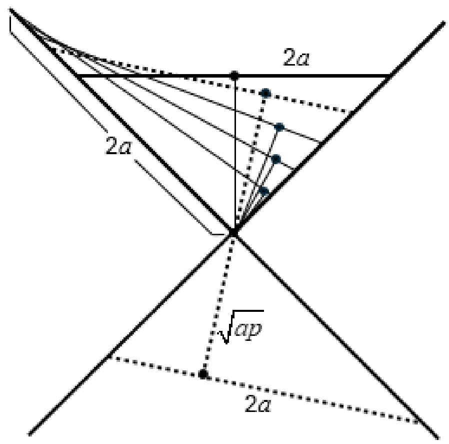

Fig. 5 Elliptical Orbits in Edge View with Equal Total Energy

At intermediate eccentricities, the orbits exhibit rotational motion about the cone axis; as $e \to 1$, the semi-latus rectum $p \to 0$, and $R = r$, recovering the rectilinear case in which the orbital plane lies along a generator of the cone. Rectilinear trajectories represent a physically realizable limiting case, straight-line paths between two bodies under gravity, and Vallado recognizes them for each orbit type.[5]

E. Orbital Plane Orientation and the Conical Frame.

The conical reference frame employs a Cartesian coordinate system (x, y, z) with the z-axis coinciding with the cone centerline. The angular momentum vector ($h = rxv$) lies on the line from the apex to point F and remains fixed in inertial space for Keplerian motion. The orbital plane intersects the cone at an angle determined by the eccentricity, and line $OF = \sqrt{ap}$ is the perpendicular distance from the apex to this plane. As shown in Fig. 2, the classical parameters of the orbit apply, and the conical parameters R and Q are sufficient to identify the satellite position since the apex angle is fixed at 90 degrees. Figure 3 shows the relationship between R and the component perpendicular to designated R'. The magnitude of R' is $R/\sqrt{2}$ for the 90-degree cone. This geometric arrangement allows complete three-dimensional orbital motion to be decomposed into two components: motion along the cone surface characterized by R, and rotation about the cone axis characterized by angle Θ. Equation (4) is a corollary to Eq. (3),

$$R'^2 = \frac{1}{2}\left(r^2 + ap\right) \tag{4}$$

V. Gauss's Law

Gauss's law for gravitation states that the total normal outward gravitational flux through a closed surface equals $-4\pi G$ times the enclosed mass [7, 8]. For a single body of mass M, substituting $\mu = GM$ gives

$$\int g \, dA = -4\pi\mu \tag{5}$$

where $\boldsymbol{g}$ is the gravitational acceleration and $\boldsymbol{n}$ is the outward unit normal on the Gaussian surface. For a sphere of radius R centered on M, the field magnitude is μ/R^2 and the surface area is $4\pi R^2$, so the integrand is constant and the R^2 factors cancel identically, confirming that the flux is $-4\pi\mu$ regardless of sphere size.

Three properties of Gauss's theorem are relevant to the conical framework. First, the enclosed mass must lie within the Gaussian surface; this paper limits application to the two-body problem, and the primary body at focus F remains enclosed for all orbital positions. Second, the theorem places no constraint on where within the surface the mass sits, so the flux argument holds across the full eccentricity range $0 < e < 1$ without modification as F moves along the major axis. Third, flux is independent of the shape and size of the Gaussian surface, permitting non-spherical geometries. This third property is the operative one for the present work. A spherical cap of half-angle Φ_c (Fig. 6) has area

$$A_{cap} = 2\pi R^2\left(1 - \cos\Phi_c\right) \tag{6}$$

and subtends solid angle $\Omega = 2\pi(1 - \cos\Phi_c)$. Because the R^2 factors cancel in the flux integral, the cap carries flux

$$\psi_{cap} = -\mu\,\Omega \tag{7}$$

independent of sphere radius. The same cancellation applies when the cap is replaced by a flat disk of circumradius $R' = R\sin\Phi_c$: the disk subtends the same solid angle and carries the same flux. The shape of the bounding surface therefore does not affect the flux, provided the conditions of Gauss's law are satisfied, and the conical surface may be evaluated in sections without requiring a fully closed surface at each step.

VI. Gauss's Law Application

Gauss's law applied to the conical reference frame with a 90° apex angle yields new results for elliptical orbits. Because flux lines follow radial generators of the cone and the R^2 cancellation established in Section V holds at every radius, the conic sector subtends a fixed solid angle $\Omega = 2\pi(1 - \cos\Phi_c)$ independent of R, and the flux through that sector is constant throughout the orbit. The following subsections derive the eccentricity–tilt relation, extend the flux result dynamically to recover Kepler's equation in logarithmic form, and present the dual-tolerance Newton-Raphson positioning scheme.

A. Unique 90-Degree Cone Frame

The tilt of the orbital plane with respect to the cone axis is denoted Φ_h, the angle between the cone axis and the line OF. It is measured toward periapsis. The angle Φ_h is determined from the edge view shown in Fig. 4. In this view the cone appears as two generators at 45° to the vertical centerline, the line $OF = \sqrt{ap}$ extends from the apex O to the focus F at angle Φ_h from the centerline, and the distance from F to periapsis P equals $a(1-e)$. In the right triangle OFP, the right angle is at F, the hypotenuse OP lies along the 45° cone generator with length $a\sqrt{(2-2e)}$, and the angle at O between the generator and OF is $(45° - \Phi_h)$. Therefore:

$$\sin\left(\pi/4 - \Phi_h\right) = \frac{a(1-e)}{a\sqrt{2-2e}} = \sqrt{\frac{1-e}{2}} \tag{8}$$

The complementary angle follows directly:

$$\cos\left(\pi/4 - \Phi_h\right) = \sqrt{\frac{(1+e)}{2}} \tag{9}$$

Apply the double-angle identity

$$\cos\left(\pi/2 - 2\Phi_h\right) = 1 - 2\sin^2\left(\pi/4 - \Phi_h\right) \tag{10}$$

and substitute Eqs. (8) and (9) to show that

$$\sin\left(2\Phi_h\right) = e \tag{11}$$

B. Gravitational Flux and the Conic Reference Frame

The conical reference frame employs two angular coordinates to describe satellite position: true anomaly θ measured in the orbital plane from periapsis, and Θ measured in the x–y plane for rotation about the cone axis. Both describe the same orbital motion in different planes, related by the tilt Φ_h. The primary mass at F is displaced from the cone apex O by $\sqrt{ap}$ along the angular momentum vector. Because the conic sector subtends the fixed solid angle $\Omega = 2\pi(1 - \cos\Phi_c)$ at every value of R, the flux through the sector is

$$\int g\, dA = -\mu\, \Omega \tag{12}$$

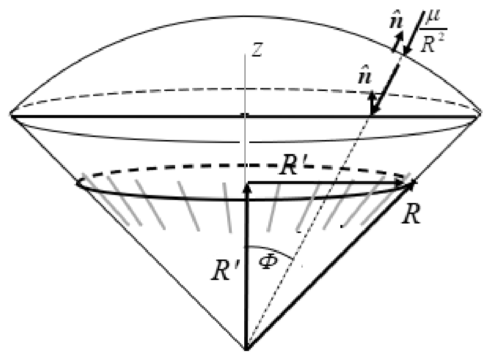

Fig. 6 Conic Sector of a Sphere with 90° Apex

C. Rectilinear Trajectories

Postulate: Rectilinear trajectories emanating from a spherical center, directed along the slant-height generators of a 90-degree cone satisfy Gauss's law evaluated at the intersection of the cone with any concentric sphere.

As noted in Section IV.D, the rectilinear case ($e \to 1$, $\Phi_h \to 45°$) has $R = r$ and no rotational component. Gauss's law applied over the full sphere recovers the standard result $\int \mathbf{g}\, dA = -4\pi\mu$, confirming the conical framework reduces correctly to the classical limit. Because the rectilinear trajectory does not close, it has no orbital period solution and is not developed further here.

D. Dynamic Extension of the Flux Integral

The flux invariance of Section VI.B establishes that Gauss's law applies at every point along the orbit. To extract a time-displacement relationship, that instantaneous result is extended by integrating the flux accumulation as the satellite advances from periapsis. Figure 7 shows the disk geometry. The annular disk at slant height R has circumradius R' and incremental width dR along the cone surface. The inner integral sweeps the circumference through azimuthal angle Θ at fixed R, yielding the factor 2π. The outer integral accumulates flux as R advances from R at periapsis to $R(E)$ and substituting $dR/dt = \dot{R}$ gives Eq. (13).

$$\Psi = \mu \sin \Phi_h \int_0^t \int_0^{2\pi} \frac{\dot{R}}{R} d\alpha \, dt \tag{13}$$

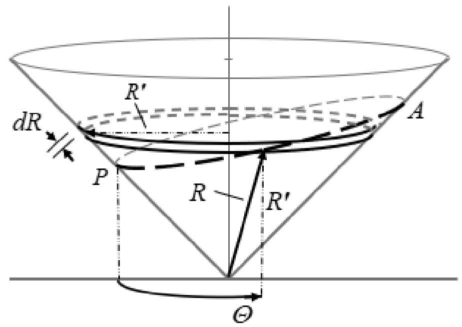

Fig.7 Disk at Slant Height R Showing Circumradius *R′*, Increment d*R*, and Azimuthal Angle *Θ*

Evaluating the inner integral over the full circumference,

$$\Psi = 2\pi \, \mu \sin \Phi_h \int_0^t \frac{\dot{R}}{R} dt \tag{14}$$

The integrand $\dot{R}/R$ is the logarithmic derivative of R, so the accumulated flux integral evaluates exactly to

$$\Psi = 2\pi \, \mu \sin \Phi_h \ln\left(\frac{R(E)}{R_P}\right) \tag{15}$$

For the Newton-Raphson positioning scheme developed in Section VI.E, it is convenient to define the logarithmic position variable $\lambda = ln[R(E)/RP]$, so that Eq. (15) shows Ψ is directly proportional to λ. The variable λ ranges from zero at periapsis to $tanh^{-1}(e)$ at apoapsis and provides a geometrically uniform measure of orbital progress along the cone surface. This result has a direct physical reading: the gravitational flux accumulated through the conic sector from periapsis to the current position is proportional to the logarithm of the slant-height ratio. At periapsis $R = R_P$ and $\lambda = 0$; at apoapsis $R = R_A$ and $\lambda = tanh^{-1}(e)$, recovering the apse-ratio identity established geometrically in Section VI.B.

To connect Eq. (15) to the orbital time history, $\dot{R}$ is expressed in terms of the eccentric anomaly E. With $R^2 = r^2 + ap$, differentiation and the standard result $\dot{r} = (\sqrt{\mu/a}) \cdot e \sin E / (1 - e \cos E)$ give

$$\dot{R} = \frac{r}{R}\dot{r} = \sqrt{\frac{\mu}{a}} \frac{e \sin E}{R/a} \tag{16}$$

Changing the integration variable from t to E using $dt = \sqrt{(a^3/\mu)}(1 - ecosE)dE$, Eq. (15) becomes

$$\ln\frac{R(E)}{R_P} = \int_0^E e \sin E' \frac{(1 - e \cos E')}{(1 - e \cos E')^2 + (1 - e^2)} dE' \tag{17}$$

This integral is evaluated in closed form by the substitution $w = 1 - ecosE'$, which maps the eccentric anomaly directly onto the R-coordinate through the relation $R^2/a^2 = w^2 + (1 - e^2)$[10], yielding

$$\ln\frac{R(E)}{R_P}=\frac{1}{2}\ln\left[\frac{(1-e\cos E)^2+(1-e^2)}{2(1-e)}\right] \tag{18}$$

Since $R^2(E)=a^2[(1-ecosE)^2+(1-e^2)]$ and $R^2{}_P=2a^2(1-e)$, Eq. (18) is identically $ln[R(E)/R_P]$, confirming self-consistency. The expression holds pointwise throughout the orbit, reducing to zero at periapsis (E = 0) and to $tanh^{-1}(e)$ at apoapsis ($E=\pi$), consistent with the apse-ratio identity.

The dynamical content of this result parallels Kepler's equation: both encode the full orbital time history parametrically through E, and both reduce to the same apse values. The conical frame provides a three-dimensional geometric home for the eccentric anomaly, complementing its classical interpretation as the parameter of the auxiliary circle in the orbital plane [9].

E. Numerical Solution for Time-Known Positioning

The inverse problem of orbital mechanics, determining satellite position from a known elapsed time, requires numerical methods because Kepler's equation is transcendental. The conical reference frame provides a natural setting for this computation, and the logarithmic structure of Section VI.D offers both a direct solution path and an independent geometric convergence check unavailable in the classical two-dimensional approach.

The classical approach solves Kepler's equation $\boldsymbol{E-e\sin E}=\sqrt{\mu/a^3}\ \boldsymbol{t}$ iteratively for E and then converts E to true anomaly θ through trigonometric inversion, which introduces additional numerical sensitivity for highly eccentric orbits where the geometry crowds near periapsis. In the conical framework, slant radius R replaces θ as the primary position variable and is recovered from a converged E by direct algebraic evaluation, eliminating the trigonometric inversion.

Given elapsed time t, the residual function for Kepler's equation is

$$f(E)=E-e\sin E-\sqrt{\frac{\mu}{a^3}}\,t \tag{19}$$

with derivative $f'(E)=1-ecosE=r/a$. Since r/a is strictly positive, $f(E)$ is monotonically increasing, and Newton-Raphson iteration converges globally. The iteration proceeds as

$$E_{n+1}=E_n-(\frac{E_n-e\sin E_n-\sqrt{\frac{\mu}{a^3}}\,t}{1-e\cos E_n} \tag{20}$$

initialized with $E_0=\sqrt{(\mu/a^3)}\ t$. At each step, the logarithmic position variable

$$\lambda_{n+1}=\frac{1}{2}\ln\left[\frac{\left(1-e\cos E_{n+1}\right)^2+\left(1-e^2\right)}{2(1-e)}\right] \tag{21}$$

is updated with E, and the slant radius is recovered as

$$R_{n+1}=R_P\,e^{\lambda_{n+1}} \tag{22}$$

where $R_P=a\sqrt{2(1-e)}$. Convergence requires dual tolerance conditions on both the Kepler residual and the logarithmic position increment:

$$\left| f\,(E_{\ \ +1}) \right| < \tau,\ E \quad \text{and} \quad \left| \lambda_{\ \ +1} - \lambda_{\ \ } \right| < \tau,\ \lambda \tag{23}$$

The dual check is the key structural difference from the classical approach. Satisfaction of the Kepler tolerance confirms that the time equation is converged; satisfaction of the geometric tolerance confirms that the solution is physically consistent with the cone geometry. These are independent conditions and combining both provides a built-in verification that the classical two-dimensional approach cannot offer. The logarithmic variable λ, ranging from zero at periapsis to $tanh^{-1}(e)$ at apoapsis, also distributes numerical resolution more evenly across the orbit than r does, which is most valuable as $e \rightarrow 1$ where classical Kepler solution requires the most iterations. Once both tolerances are satisfied, the full orbital state is recovered from the converged E and R. The orbital radius and true anomaly follow from the polar equation for a conic section.

$$\cos\theta = \frac{1}{e}\left(p/r - 1 \right) \tag{24}$$

and the three-dimensional position in the conical frame is given by the cylindrical coordinates

$$z = R\cos\Phi_c, \quad \rho = R\sin\Phi_c = R' \tag{25}$$

where z is along the cone axis and ρ is the perpendicular distance from it. Because the cone half-angle $\Phi_c = 45°$ is fixed, $z = \rho = R'$ at every point along the orbit, consistent with $R^2 = r^2 + ap$, or equivalently $2R'^2 = r^2 + ap$. The precision of the solution is controlled by the choice of $\tau_E$and , which may be set independently. Near periapsis, where small changes in E produce large changes in R, the geometric tolerance τ_λ provides a more sensitive criterion; near apoapsis, τ_E, is primary. Selecting tolerances adaptively based on the current value of λ relative to $tanh^{-1}(e)$ is a natural extension that the logarithmic formulation makes straightforward.

The logarithmic variable also suggests a natural node-placement strategy for table-lookup positioning, useful when rapid repeated evaluations are required across many candidate geometries. Uniform spacing in R produces node spacing in r that is finer in the lower arc precisely where high-eccentricity trajectories create the greatest interpolation challenge. It is a direct structural consequence of $R^2 = r^2 + ap$ rather than parameter tuning. Numerical verification for a representative high-eccentricity lofted intercept trajectory is given in the Appendix. For a representative high-eccentricity lofted intercept ($e = 0.996$, $\gamma = 85°$), R-frame node placement reduces TOF interpolation error at the target by roughly a factor of five relative to uniform-time Kepler nodes (2.1 s vs. 11.1 s); the full numerical comparison is given in the Appendix."

VII. Conclusion

Three results have been developed for two-body orbital motion analyzed within a three-dimensional conical reference frame having a 90-degree apex angle and its apex at the center of the gravitational field.

A. Tilt angle. The angle Φ_h of the orbital plane relative to the cone axis satisfies $sin(2\Phi_h) = e$, providing a direct geometric encoding of eccentricity that is intrinsic to the frame and requires no reference to the orbital plane. This result emerges from the edge view geometry of the 90-degree cone and the standard ellipse parameters and does not appear to have been previously stated in this form.

B. Logarithmic flux. Apply Gauss's law for gravitation to the conical surface to yields a logarithmic flux integral that connects pointwise to Kepler's equation through the eccentric anomaly E. This establishes a three-dimensional geometric interpretation of that classical result, complementing its traditional two-dimensional interpretation as the parameter of the auxiliary circle in the orbital plane.

C. Numerical Solution. The logarithmic structure supports a Newton-Raphson positioning scheme with dual convergence tolerances, one on the Kepler residual and one on the logarithmic position variable providing an independent geometric consistency check that is unavailable in the classical two-dimensional approach.

The conical reference frame developed here applies to bound elliptical orbits. Several extensions present themselves as directions for further work. The framework may generalize to hyperbolic trajectories, where $e > 1$ and the cone geometry would require reexamination of the $sin(2\Phi_h) = e$ result. The dynamic conformance models introduced in Ref. [5] offer a further extension, potentially transforming the static flux result into a time-evolving dynamical statement. The intersection of two cones, each associated with a distinct orbit sharing a common focus, may provide geometric insight into orbital transfer problems. Geodesic paths on the cone surface represent an additional avenue connecting the geometric framework to variational methods in orbital mechanics.

References

[1] "Apollonius of Perga," *New World Encyclopedia*, https://www.newworldencyclopedia.org/entry/Apollonius_of_Perga#Conics (retrieved March 2026).
[2] Bate, R. R., Mueller, D. D., White, J. E., and Saylor, W. W., *Fundamentals of Astrodynamics*, 2nd ed., Dover Publications, New York, 2020.
[3] Curtis, H. D., *Orbital Mechanics for Engineering Students*, 3rd ed., Elsevier Butterworth-Heinemann, Oxford, 2013.
[4] Vallado, D. A., *Fundamentals of Astrodynamics and Applications*, 2nd ed., Microcosm Press, El Segundo, CA, 2004.
[5] May, D. H., "Integrated Orbital Motion Equations with Conformance Models," Paper AIAA-99-4060, AIAA Guidance, Navigation, and Control Conference, Portland, OR, August 1999.
[6] May, D. H., "Modeling Orbital Motion in a Circular Conic Reference Frame," Paper AIAA 2022-1431, AIAA SciTech 2022 Forum, San Diego, CA, January 2022.
[7] Halpern, J., "54.7: Gauss's Formulation," *Physics LibreTexts*, https://phys.libretexts.org/Courses/Prince_Georges_Community_College/General_Physics_I%3A_Classical_Mechanics/54%3A_Gravity/54.07%3A_Gausss_Formulation (retrieved February 2026).
[8] Tatum, J. B., "5.5: Gauss's Theorem," *Celestial Mechanics*, Physics LibreTexts, https://phys.libretexts.org/Bookshelves/Astronomy__Cosmology/Celestial_Mechanics_(Tatum)/05%3A_Gravitational_Field_and_Potential/5.05%3A_Gauss's_Theorem (retrieved February 2026).
[9] May, D. H., "Orbital Motion Equations with Dynamic Models," Paper AAS 05-354, AAS/AIAA Astrodynamics Specialist Conference, Lake Tahoe, CA, August 2005.
[10] Zwillinger, D., *Standard Mathematical Tables and Formulae*, 30th ed., CRC Press, New York, 1996.

The author thanks Claude AI (Anthropic) for assistance in developing and refining the mathematical presentation.

VIII. Appendix: Numerical Positioning and R-Frame Interpolation

A. Example Trajectory

The numerical example uses a lofted intercept trajectory with booster separation conditions r_1= 6,578 km (200 km altitude), v_1 = 7.20 km/s, and loft angle γ = 85°. These yield the orbital elements shown in Table A-1. The target is in a circular orbit at r_{tgt} = 9,025.8 km (altitude 2,647.8 km), representative of a lofted intercept trajectory in the class examined by Bate, Mueller, and White (pp 223-226) [2]. Eccentricity e = 0.99627 places this orbit well into the high-eccentricity regime, where $\lambda_{max} = tanh^{-1}(e) \approx \pi$ as a coincidence of this trajectory rather than a general result.

Table A-1. Orbital elements for the 85° loft angle case.

Parameter	Symbol	Value
Semi-major axis	a	5,747 km
Eccentricity	e	0.99627
Apogee radius	r_A	11,474 km (5,096 km altitude)
Target radius	r_{tgt}	9,025.8 km (2,648 km altitude)
TOF, launch to target (exact)	t_{exact}	436.82 s

B. Results

Two node-placement schemes are compared for interpolated time-of-flight (TOF) to the target. The Kepler scheme places eleven nodes at uniform time intervals from launch to apogee and locates r at each by Newton–Raphson inversion of Kepler's equation. The R-frame scheme places eleven nodes at uniform intervals of slant radius R, recovering r at each node directly from $r = \sqrt{R^2 - ap}$ with no iteration required. In both cases, TOF at the target is estimated by linear interpolation between the two bracketing nodes. Table A-2 gives the interpolated TOF at r_{tgt} for both schemes.

Table A-2. TOF at target radius: interpolation comparison.

Method	Interpolated TOF (s)	Error vs. exact (s)
Exact Kepler (reference)	436.820	—
R-frame interpolation	434.677	−2.143
Kepler uniform-time interpolation	447.953	+11.133

The Kepler interpolation error is more than five times larger than the R-frame error, a direct consequence of the uneven Kepler node spacing: uniform time steps cluster nodes near apogee, where the satellite moves slowly, leaving a 739 km gap in r across the lower arc where the target falls. At the target's circular velocity of 6.65 km/s, the 13.3 s difference between the two interpolated TOFs corresponds to an along-track discrepancy of roughly 88 km, an upper bound on the range error attributable to node-placement choice alone, and operationally significant for an intercept problem.

This is a structural result, not an artifact of parameter tuning. Because $R^2 = r^2 + ap$, uniform spacing in R automatically produces finer spacing in r wherever the trajectory is steep and near-radial. It is in the orbit segment where r is still small and changing rapidly, and where high-eccentricity geometry creates the widest Kepler time steps. In the example shown here, that error falls within this steep, near-radial segment rather than being spread evenly across the trajectory. The R-frame nodes are also computed without iteration ($r \rightarrow E \rightarrow t$), making the scheme simultaneously more accurate at this target altitude and computationally simpler than the Kepler approach.

The advantage persists across loft angle. Table A-3 gives the interpolation error for both methods across five loft angles from $\gamma = 70°$ to $\gamma = 90°$ ($e = 0.941$ to $e = 1$), shown in Fig. A-1. The Kepler error grows monotonically with eccentricity, from 1,835 ms to 3,793 ms, while the R-method error is non-monotone, falling to a minimum of 34 ms at $\gamma = 80°$ before rising to 452 ms at $\gamma = 90°$. At $\gamma = 90°$ the orbit is rectilinear ($e = 1$, $ap = 0$), where the R-method reduces to uniform steps in r and the two schemes converge in character — confirming that the R-frame formulation degrades smoothly to the classical result in this limiting case.

Table A-3. TOF interpolation error comparison across loft angles (N = 10 nodes, r_{tgt} = 9,000 km)

γ	e	Exact TOF (s)	Kepler Error (ms)	R-method Error (ms)
70°	0.941	461.773	1,835	1,506
75°	0.967	446.847	2,985	747
80°	0.985	436.742	3,519	34
85°	0.996	430.886	3,674	341
90°	1.000	428.967	3,793	452

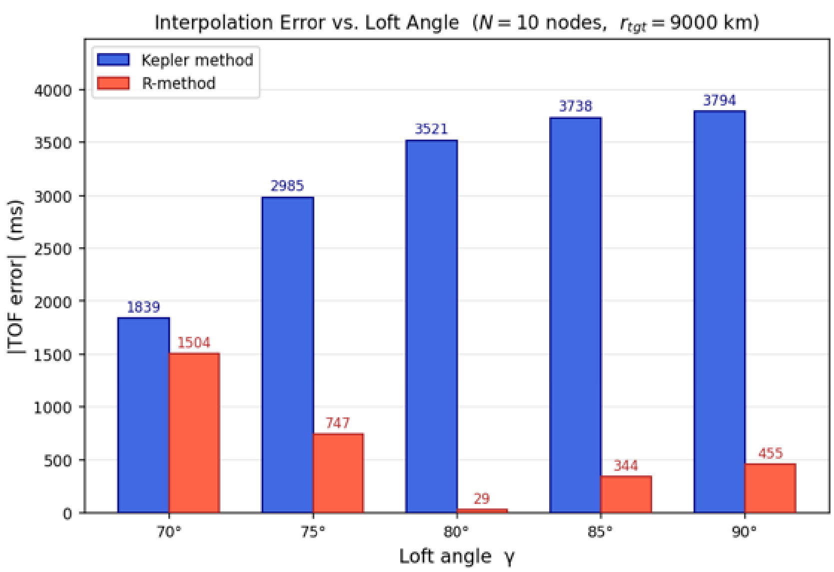

Fig. A-1. TOF Interpolation Error vs. Loft Angle for the Kepler and R-Frame Methods

Whether the R-method advantage persists across a wider range of node counts, target altitudes, and orbit families is a question for further study; the present example demonstrates the principle for the high-eccentricity regime that is the focus of this paper.